Proceedings of the 7th International Conference on Geotechnical and Geophysical Site Characterization (ISC)
June 18-21, 2024, Barcelona, Spain

On the determination of soil deformation modulus by means of a penetrometer

Sébastien H.E. Volcy[1*], *Luc* Sibille[1], *Bruno* Chareyre[1], *Christophe* Dano[1] and *Hamid* Hosseini-Sadrabadi[2]

[1] *Univ. Grenoble Alpes, CNRS, Grenoble INP, 3SR F-38000 Grenoble, France*
[2] *Equaterre: Geotechnical Design Office, Annecy, France*
6 Rue de l'Euro, 74960 Meythet
[*] *sebastien.volcy@3sr-grenoble.fr*

ABSTRACT. Classical Cone Penetration Test (CPT) or CPTu (when water pore pressure is also measured) can provide so far only strength parameters of soils, specifically the tip resistance and the lateral friction. This article presents the numerical simulation in a (virtual) calibration chamber, using the Discrete Element Method (DEM), of a CPT-based test proposed in the quest for possibilities to determine soil deformability parameters as well. It is a non-standard test characterized by force-controlled cycles applied to the penetrometer tip that is movable independently of the penetrometer body. Very small irreversible displacements of the tip are observed over the first cycles whose amplitudes span a region of low fractions of the tip resistance, that is subsequently assimilated to a pseudo-elastic domain within which, deformation moduli can be derived from the slopes of the force-displacement curve properly interpreted. Results also reveal a loading level beyond which, these slopes and the corresponding deformation moduli, significantly decrease while the irreversible displacements of the tip increase substantially.

Keywords: Cyclic CPT; Discrete Element Method; Deformability Modulus; pseudo-Elastic Domain.

1. Introduction

The classical Cone Penetration Test (CPT) consists of pushing into a soil, a conical tip, topped by a train of rods, with a velocity of 1 to 2 cm/s, while recording at the same time the tip resistance q_c, the sleeve friction f_s and potentially the pore water pressure u, in which case the test is called a CPTu. As such, the soil under the tip is at failure, which renders the test inappropriate in the search for soil deformability parameters. As raw informations, it can provide only strength parameters (Reiffsteck et al., 2007).

Nonetheless, works have been undertaken on the possible derivation of soil deformation modulus from CPT data, either through empirical or semi-empirical relations between the tip resistance q_c and some usual deformation moduli as presented in Table 1, or through CPT-based tests. The latter includes for instance the Cone Loading Test (CLT) proposed by Faugeras (1979) and successively further developed by Faugeras et al. (1983), Zhou (1997), Arbaoui et al. (2006) and Reiffsteck et al. (2007).

The CLT consists in interrupting the penetration of the penetrometer at a certain depth, waiting for the dissipation of excess pore pressure if the soil is not dry, and axially loading the tip of the penetrometer gradually in successive steps until the soil underneath fails.

Table 1. Some proposed empirical relations between some deformation moduli and the tip resistance q_c in sands; E_{oed} : oedometric modulus, E_M : pressuremeter modulus.

E_{oed}/q_c	2.5<.<3.5	(Schmertmann, 1978)
	1.5	(Costet et Sanglerat, 1981, 1983)
	1<.<2	(Bachelier et Parez, 1965)
E_M/q_c	3<.<4	(Kérisel, 1958) d'après Cassan (1978)
	1.1	(Van Wanbecke, 1962) d'après Cassan (1978)

Hereafter, is presented the numerical modeling of a new CPT-based test developed by Equaterre company (Riegel, 2017). The methodology is a non-standard one, as the tip is movable alone, thus allowing cycles, either force-controlled or displacement-controlled, to be applied to the tip only, i.e while the remaining body of the penetrometer being on rest. First, alike the CLT, there is a phase of classical monotonic penetration of the tip. However, once a certain depth is reached, the tip resistance q_c is recorded and the tip is unloaded, down to a fraction of q_c, enough to keep the soil beneath it in compression. Then, force-controlled cycles with increasing amplitudes are applied to the tip.

This methodology offers the opportunity to investigate different stress levels underneath the tip in regard to their influence on the soil deformability modulus. It presents also the advantage, in real experiments, to avoid the friction between the soil and the system moving the tip (the internal rods), which runs inside the body of the penetrometer (the train of bars) as shown in Fig. 1. By this way, friction between the soil and the body of the penetrometer has no influence on the test results.

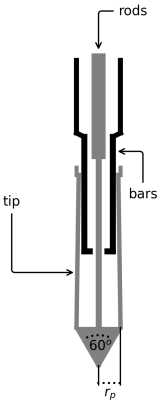

Figure 1. The geometry of the tip.

2. Numerical model

2.1. Numerical method

The Discrete Element Method as invented by Cundall and Strack (1979) is used for the modeling. A 3D assembly of spheres represents the solid skeleton of the soil, whose mechanical behaviour stems from laws governing the contacts between the spheres.

As shown in Fig. 2, any contact is modeled as a set of a normal spring, a tangential spring, and a rotational spring, whose stiffnesses k_n, k_t and k_r, are used to compute the contact forces and torques between the grains being involved in the contact, knowing their kinematic variables. As defined in Equation 1, these stiffnesses are normalized by the radii R_1 and R_2 of the grains in contact so that the macroscopic response of the system does not depend on the grains size. Such a choice is justified by the specific discretization approach of the soil adopted here and presented in section 2.2.

$$k_n = 2E_c\frac{R_1R_2}{R_1+R_2},\ k_t = \alpha_t k_n,\ k_r = \alpha_r k_t R_1 R_2 \quad (1)$$

with E_c being the characteristic modulus of the contact and, α_t and α_r, two dimensionless coefficients, related to the shear and the rolling stiffnesses respectively.

In addition to these stiffnesses, the contact friction angle ϕ_c and the rolling friction coefficient η_r bring the number of the model parameters to 5. As the model is initially built in order to simulate the test on real sands, there is no cohesion at the contacts, which are then purely frictional.

The introduction of rolling resistance at the contacts brings realism to the model as it prevents excessive rotations of the spheres idealizing the soil grains. As a matter of fact, in real soils, the particles shape that is often far from being spherical has a strong influence on their rotation.

The contact laws can be written as:

$$\vec{F}_n = k_n\delta_n\vec{n}, \quad (2a)$$

$$\Delta\vec{F}_t = -k_t\Delta\delta_t\vec{t},\ ||\vec{F}_t|| \leqslant ||\vec{F}_n||\tan\phi_c \quad (2b)$$

$$\Delta\vec{M}_r = -k_r\Delta\vec{\Theta}_r,\ ||\vec{M}_r|| \leqslant \eta_r||\vec{F}_n||\min(R_1,R_2) \quad (2c)$$

with $\vec{F}_n$ and $\vec{F}_t$, the normal and the tangential components of the contact force, $\vec{M}_r$, the rolling moment, $\vec{n}$, the unit vector normal to the contact plane, $\vec{t}$, the unit vector perpendicular to $\vec{n}$ and lying in the contact plane. As to δ_n, $\Delta\delta_t$ and $\Delta\vec{\Theta}_r$, they are respectively the normal overlap, the incremental relative tangential displacement and the incremental relative tangential rotation between two grains of radii R_1 and R_2.

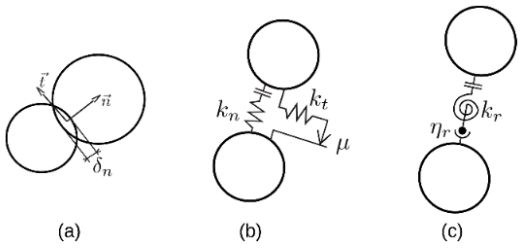

Figure 2. Modeling of a contact between two grains.

2.2. Simulation setup

The numerical setup includes:

- a penetrometer modeled as spheres that are clumped together in a way that reproduces its actual geometry shown in Fig. 1 with a radius r_p and an apex angle of 60^o. Actually, two clumps, as clearly discriminated in Fig. 3, that can move relatively to each other are used to reproduce the mechanism of the moveable tip: one represents the penetrometer tip and the other, the remaining body of the penetrometer.

Figure 3. The tip as modeled.

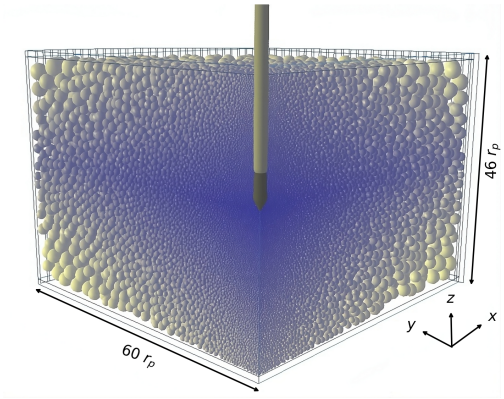

Figure 4. The numerical model after compaction. The size of the spheres increases with their distance from the tip.

- a soil whose grains are modeled as standalone spheres. They are spatially distributed according to their size using the particle refinement method as in (Hosseini-Sadrabadi and al., 2018) and (Abdallah and al., 2022), which is characterized by the increase of the size of the grains with their distance from the singularity, materialized here by the tip. In other words, a large number of small size spheres are located around the tip and a few large ones away, as can be seen in Fig. 4. This approach cuts computational costs while ensuring reliable results.

- a calibration chamber containing the soil sample over which the test is carried. For axisymmetric reasons, it is represented as one-fourth of a cylinder bordered by 5 walls: 2 vertical ones, 1 cylindrical one and 2 horizontal ones. This geometrical simplification is inspired from Abdallah and al. (2022) who, modelling the pressuremeter test, adopted the same geometry for the chamber, after comparisons of the results with the ones obtained with a model representing the chamber as a complete cylinder.

  In order to minimize boundary effects, the chamber radius r_c is taken as $60\ r_p$. The top and the bottom walls are placed, respectively at $20\ r_p$ and $26\ r_p$ from the tip (Fig. 4).

3. Methodology

3.1. Simulation of the initial state

The sample preparation is performed in 4 steps:

1. First, a very loose cloud of spheres (with no interparticle contacts) is generated, given the required particle size distribution.

2. Secondly, the so-generated particles are steadily grown. The contact friction angle ϕ_c is tuned to a certain value ϕ_{comp} to reach a target porosity n at the end of this radii expansion phase. The lower ϕ_{comp}, the easier for the grains to move relatively to each other , the denser the sample eventually.

3. Then, the isotropic state of stress induced by the previous step is removed by slightly downsizing the spheres. This results in a decrease in the mean pressures on the walls.

4. Finally, an œdometric compression phase completes the sample preparation. It consists of stress-controlling the top and the bottom walls until the vertical stress on them reaches a desired value σ_v. At the end of this final step, the contact friction angle is set to the nominal value used for the simulation, greater than ϕ_{comp}.

   Figure 4 presents the model after the preparation of the numerical soil sample. As observed, the sample is prepared with the tip inside the chamber. This choice is made to cut the computational cost in time

that the penetration of the tip from outside the chamber would generate. Yet, a short monotonic penetration up to a depth z_p is simulated prior to the cycles, in order to reproduce around the tip a state of stress that would be representative of a previous conventional cone penetration. The depth test z_p is taken below the critical depth, defined as the depth at which the tip resistance q_c is constant.

3.2. Loading of the tip

As described in section 1, the course of the simulated test involves two types of loading of the tip. The monotonic loading is achieved by assigning to the tip a downward velocity v_m. This stage lasts until the tip reaches the depth z_p at which the cyclic test is done.

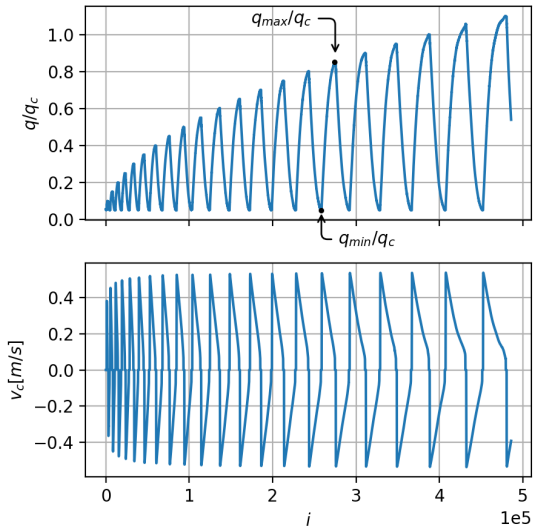

Figure 5. The assigned velocity v_c to the tip and the resulting stress q the soil exerts on it, both versus the number of iterations i, during the cyclic loading. The normalizing parameter q_c is the tip resistance recorded at the end of the previous monotonic penetration phase.

Concerning the cyclic loading, its principle is exactly the same as for the monotonic loading, except that the sign of the velocity v_c is reversed when necessary; i.e when the stress q on the tip reaches the prescribed extreme values q_{min} and q_{max} on the considered cycle.

Figure 5 presents the evolution of the velocity as assigned to the tip and the resulting stress on it during the cyles, versus the number i of iterations. As shown, the amplitudes of the cycles increase over time; the minimum value q_{min} is fixed (here taken on a lump-sum basis equal to 5% of the tip resistance q_c) while the maximum value is increased by a constant quantity one cycle after the other.

4. Results and discussions

In this section, are discussed the results of three simulations, referred to as s_1, s_2 and s_3 in what follows. The parameters relative to the soil used for these simulations are given in Table 2.

Table 2. Simulation parameters and some results. The normalizing parameter r_p is the tip radius.

Simulation	s_1	s_2	s_3
ϕ_{comp} $(^o)$	10	15	25
n	0.44	0.46	0.50
E_c (N/m^2)	3×10^7		
α_t	0.33		
α_r	5.0		
ϕ_c $(^o)$ (nominal value)	30		
Cohesion c	0		
η_r	0.35		
v_m (m/s)	1		
σ_v (kPa)	100		
N: number of soil particles	115 003		
z_p/r_p	4		
q_c (MPa)	4.2	3.5	2.6

Figure 6 shows the soil response to the classical monotonic penetration of the tip, the earliest phase of the simulation, as described in the methodology presented in section 1. As shown, the depth z_p, taken as 4 times the tip radius to perform the cyclic loading is correct, as the tip resistance q_c is constant below it.

In Fig. 7 is presented the response in displacement of the tip to the cyclic loading shown in Fig. 5 (top), with a zoom on the penultimate cycle. Over this cycle, as for any other cycle, are defined the secant stiffness as the slope S_c of the line (AB) and the irreversible displacement z^* of the tip represented by the segment $[AC]$.

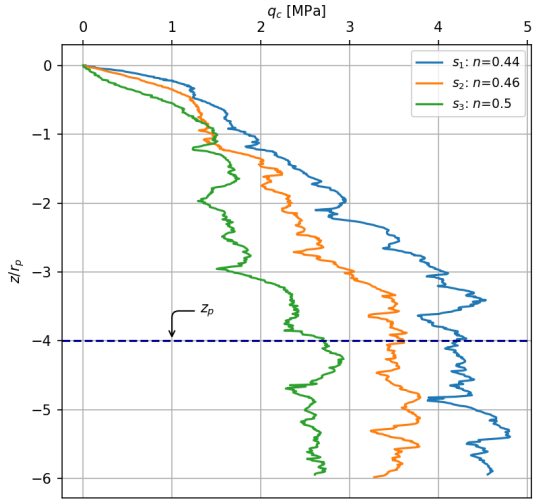

Figure 6. The soil response to the monotonic penetration of the tip. The normalizing parameter r_p is the tip radius.

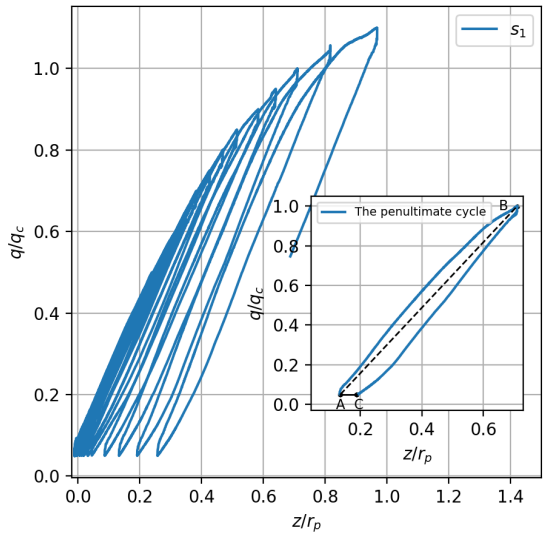

Figure 7. The stress q on the tip versus its displacement during the cyclic loading. The normalizing parameters r_p and q_c are the tip radius and the tip resistance recorded at the end of the previous monotonic penetration phase.

As it can be observed over the first cycles, characterized by low amplitudes relatively to the tip resistance q_c, the secant slopes barely differ from each other and the tip returns to almost its original position, at the end of a cycle. For conciseness' sake, the response is presented for the simulation s_1 only. But as shown by the other results, the simulation is well reproducible.

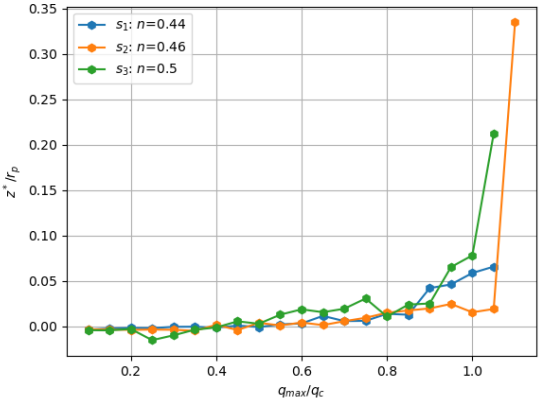

Figure 8. The irreversible displacements z^* of the tip versus the maxima of stresses q_{max} exerted on it over the cycles.

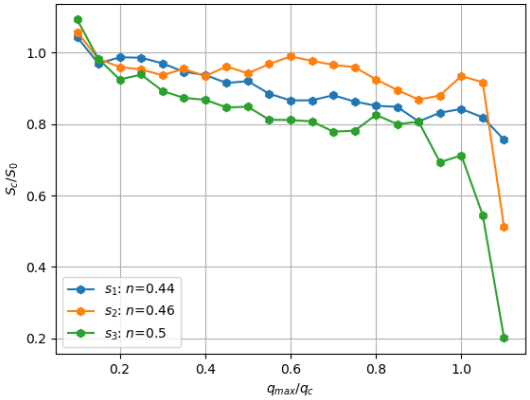

Figure 9. The secant slopes versus the maxima of stresses q_{max} exerted on it over the cycles.

Figure 8 shows the irreversible displacements z^* of the tip normalized by its radius r_p, versus the maxima of stresses q_{max} reached over the cycles normalized by the tip resistance q_c. In all cases, the observed irreversible displacements are very small over the first cycles, until a stress point (defined by $q_{max}/q_c \simeq 80\%$) beyond which they begin to be significant. Relatively to the tip resistance q_c, this stress point representing a pseudo-elastic limit is high. This result suggests a relative stress bounding the service limit state, which is greater than the one prescribed by conservative practices.

In parallel, Fig. 9 shows the evolution of the secant slopes S_c, normalized by the mean, S_0, of the secant slopes computed over the first three cycles, versus the maxima of stresses q_{max} reached over the cycles normalized by the tip resistance q_c. A small degradation of S_c, as it loses less

than 20% of its initial value even after being loaded at 60% of the tip resistance q_c is observed.

5. Conclusion

A discrete model of a non-standard CPT-based test has been presented to assess soil deformability prior to failure. Over the range of stresses lower than eight-tenths of the tip resistance q_c, only small irreversible displacements of the tip were observed. Moreover, within this stress region assimilated to a pseudo-elastic domain, the relationship between the tip displacement z and the stress q is almost linear; suggesting then a possibility to determine a deformation modulus of the soil.

Such a test is then designed for the determination of soil deformability parameters, in addition to the strength ones provided by the usual CPT. As such, a penetrometer cone could provide data for the purpose of both Ultimate Limit State (ULS) and Service Limit State (SLS) analysis of a foundation; the ULS analysis to ensure the foundation does not ruin by failure of the soil bearing it, the SLS analysis, to design the foundation against excessive settlement and rotation.

Similar results are obtained in real experiments carried out on Fontainebleau GA39 sand according to this same methology, in a physical calibration chamber and with a movable cone tip penetrometer. This reflects the ability of the model to reproduce the experiment and weighs in favor of its validation.

References

Abdallah, A., Hosn, R. A., Tfaily, B. A., and Sibille, L. (2022). Identifying parameters of a discrete numerical model of soil from a geotechnical field test. European Journal of Environmental and Civil Engineering, 27, pp. 2228–2247.

Arbaoui, H., Gourvès, R., Bressolette, P., Bodé, L. Mesure de la déformabilité des sols in situ à l'aide d'un essai de chargement statique d'une pointe pénétrométrique. Measurement of in-situ soil deformability through a static cone penetrometer test (English translation). Canadian geotechnical journal 43, pp. 355–369, 2006. https://doi.org/10.1139/t06-013

Bachelier, M., Parez, L. Contribution to the study of soil compressibility by means of a cone penetrometer, in: Proceedings 6th International Conference on Soil Mechanics and Foundations Engineering, Montreal, Canada, 1965, pp. 3-7.

Cassan, M., Cambefort H. Les essais in situ en mécanique des sols, Eyrolles, France, 1978.

Costet J., Sanglerat G. Cours pratique de mécanique des sols 1- Plasticité et calcul des tassements, 3rd ed., Dunod, France, 1981.

Costet J., Sanglerat G. Cours pratique de mécanique des sols 2- Calcul des ouvrages, 3rd ed., Dunod, France, 1985.

Cundall, P.A., Strack, O.D. A discrete numerical model for granular assemblies. Geotechnique 29, pp. 47–65, 1979.

Faugeras, J.C. L'Essai de Compressibilité des sols au pénétromètre statique et son interprétation sur modèle analogique. Ph.D. thesis, Université Paul Sabatier de Toulouse, 1979.

Faugeras, J.C, Fortuna, G., Gourvès, R. Mesure de la compressibilité des sols à l'aide du pénétromètre statique. Soil compressibility measurement by static penetrometer (English translation). In: Proceedings/Soil and rock investigations by in situ testing, international symposium 27, Paris, France, 1983, pp. 269-274.

Kérisel, J. La mécanique des sols: recherches et investigations récentes. Soils mechanics: recent research and investigations (English translation). In: Travaux 287, 1958, pp. 874-878.

Reiffsteck, P., Arbaoui, H., Gourvès, R., Bacconnet, C., Goddé, E., van de Graaf, H., 2007. Détermination de modules de déformation par chargement de pointe pénétrométrique. Determination of deformation modulus using loading test of cone penetrometer (English translation). In: 14th European Conference on Soils Mechanics and Geotechnical Engineering, Madrid, Spain, 2007, pp. 1667-1672.

Riegel, P. Pénétromètre statique pour l'évaluation du caractère liquéfiable d'un sol et procédés associés. Dépot de brevet, France, FA841687, 2017.

Sadrabadi, H., Chareyre, B., Sibille, L., and Riegel, P. Modélisation du pénétromètre statique (CPT) en condition saturée: un modèle numérique discret avec couplage fluide-solide. Modelling of the cone penetration test (CPT) in saturated condition: a discrete numerical model with fluid-solid coupling (English translation). In: 9èmes Journées Nationales de Géotechnique et de Géologie de l'Ingénieur-JNGG2018, Champs-sur-Marne, France, 2018.

Schmertmann, J.H. Guidelines for cone penetration test, Federal Highway Administration (FHWA), Florida, USA,1978.

Van Wambecke, A. Méthodes d'investigation des sols en place, étude d'une campagne d'essais comparatifs. In situ soils investigation methods, study of a comparative tests campaign (English translation). In Sols-Soils 2, pp. 9-18, 1962.

Zhou, S. Caractérisation des sols de surface à l'aide du pénétromètre dynamique léger à énergie variable type "panda". Ph.D. thesis, Clermont-Ferrand 2, 1997.